Numerical investigations on the influence of 3D frictional crack surface interaction

W. Weber[1], K. Willner[1], P. Steinmann[1] and G. Kuhn[1]

[1] Chair of Applied Mechanics, University of Erlangen-Nuremberg, Egerlandstraße 5, 91058 Erlangen, Germany.

wilhelm.weber@LTM.uni-erlangen.de

ABSTRACT. *The influence of the 3D frictional crack surface interaction on the fracture mechanical parameters as well as on the crack path is investigated numerically. For the solution of the boundary value problem the 3D dual boundary element method in terms of the discontinuous formulation is utilized. This method is especially suited for contact problems because it deals directly with the discontinuities at the crack surfaces. The contact problem is solved by the application of a penalty method. Coulomb's frictional law is utilized for the consideration of the dissipative nature of frictional contact. For discrete steps within one load cycle the stress intensity factors are determined by an extrapolation procedure from the stress field. Based on the analysis of a load cycle, the cyclic stress intensity factors are obtained. For the simulation of crack propagation an implicit integration scheme of a crack propagation law implemented in terms of a predictor-corrector scheme is applied. The influence of the crack surface roughness is shown by numerical examples.*

INTRODUCTION

For a better understanding of the behavior of cracks the numerical simulation of 3D fatigue crack growth is a useful tool. Especially for mixed mode problems crack surface interaction has to be taken into account within the simulation procedure. Due to the nonlinear nature of crack growth an incremental procedure has to be applied.

The boundary element method (BEM) is especially suited for the solution of linear-elastic stress concentration problems. For cracked structures a special formulation namely the 3D dual boundary element method (Dual BEM) [1] in terms of the dual discontinuity method (DDM) [2] is applied. Moreover, by the application of the DDM the discontinuities of the displacements and tractions are utilized as variables at the crack, which are exactly the required variables for the consideration of crack surface contact.

Then, the SIFs as well as the T-stresses are evaluated for discrete points along the crack front by an extrapolation method at each discrete time step of the stress analysis. The optimized evaluation of very accurate SIFs along the crack front is done from the numerical stress field by a regression technique controlled by the standard deviation [3].

The analysis of the time steps of a characteristic load cycle yields the cyclic fracture mechanical parameters.

A 3D crack growth criterion [4] is evaluated for the determination of the crack extension and the crack deflection. The maximum tangential stress (MTS) criterion [5,6] has been established for the calculation of the kink angle. The crack extension results from the evaluation of a crack propagation rate formulation. In case of mixed mode problems an equivalent cyclic SIF is required. This value is determined by the criterion of the maximum energy release rate [7].

Starting from an initial crack front a new one can only be predicted in a linear way. For the reduction of the linearization error, corrector steps are following a predictor step [4]. Furthermore, an optimization of the new crack front with respect to its location and shape is obtained.

STRESS ANALYSIS

The boundary value problem of the cracked domain cf. Fig. 1 is solved by the 3D dual boundary element method (3D Dual BEM) [1] in terms of the dual discontinuity method (DDM) [2]. The general time dependency of the contact problem is considered by the utilization of a rate formulation.

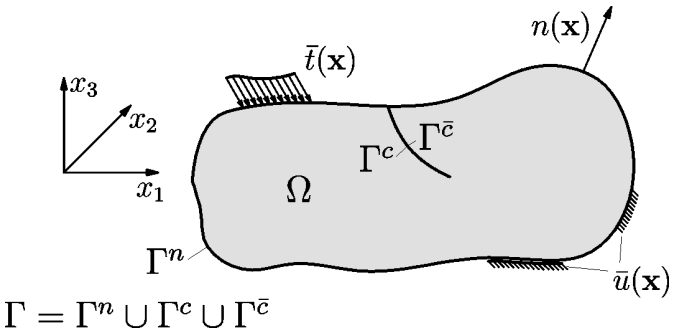

Figure 1. Sketch of the boundary value problem.

The domain $\Omega \in \Re^3$ is assumed to be homogeneous and isotropic with linear elastic material behavior. The whole boundary Γ of the domain Ω consists of the normal boundary Γ^n and the coincident crack surfaces Γ^c and $\Gamma^{\bar{c}}$, which only differ in the opposite normal direction. Along the boundary Γ Dirichlet and Neumann boundary conditions are prescribed.

For separating the coincident crack surfaces the dual discontinuity method is applied. Within this method the discontinuities of the displacement rates $\dot{\hat{u}}_i^c = \dot{u}_i^c - \dot{u}_i^{\bar{c}}$ and the traction rates $\dot{\hat{t}}_i^c = \dot{t}_i^c + \dot{t}_i^{\bar{c}}$ are introduced as new variables at the crack. By the utilization of the symmetric properties of the kernel functions, all quantities of one of the coinci-

dent crack surfaces are eliminated and only the remaining crack surface (e.g. Γ^c) has to be considered within a boundary element analysis.

After the discretization of the boundary the relevant boundary integral equations (BIEs) are evaluated in the framework of a collocation procedure. For points ξ at the normal boundary the strong singular displacement rate BIE

$$c_{ij}(\boldsymbol{\xi})\,\dot{u}_j^n(\boldsymbol{\xi}) = \int_{\Gamma^n} \left[U_{ij}(\boldsymbol{\xi},\boldsymbol{x})\,\dot{t}_j^n(\boldsymbol{x}) - T_{ij}(\boldsymbol{\xi},\boldsymbol{x})\,\dot{u}_j^n(\boldsymbol{x})\right]\,d\Gamma^n(\boldsymbol{x}) + \int_{\Gamma^c} \left[U_{ij}(\boldsymbol{\xi},\boldsymbol{x})\,\dot{\hat{t}}_j^c(\boldsymbol{x}) - T_{ij}(\boldsymbol{\xi},\boldsymbol{x})\,\dot{\hat{u}}_j^c(\boldsymbol{x})\right]\,d\Gamma^c(\boldsymbol{x}) \quad (1)$$

is evaluated. At the considered crack surface the hypersingular traction rate BIE

$$\dot{t}_j^c(\boldsymbol{\xi}) = \frac{1}{2}\dot{\hat{t}}_j^c(\boldsymbol{\xi}) + \int_{\Gamma^n} \left[\bar{U}_{ij}(\boldsymbol{\xi},\boldsymbol{x})\,\dot{t}_j^n(\boldsymbol{x}) - \bar{T}_{ij}(\boldsymbol{\xi},\boldsymbol{x})\,\dot{u}_j^n(\boldsymbol{x})\right]\,d\Gamma^n(\boldsymbol{x}) + \int_{\Gamma^c} \left[\bar{U}_{ij}(\boldsymbol{\xi},\boldsymbol{x})\,\dot{\hat{t}}_j^c(\boldsymbol{x}) - \bar{T}_{ij}(\boldsymbol{\xi},\boldsymbol{x})\,\dot{\hat{u}}_j^c(\boldsymbol{x})\right]\,d\Gamma^c(\boldsymbol{x}) \quad (2)$$

is taken into account. Therewith the unknown boundary values at the outer boundary and the displacement discontinuities at the crack can be determined if the crack surface belongs to the Neumann boundary. For the determination of the actual displacements at the crack surface the displacement rate BIE

$$\dot{u}_j^c(\boldsymbol{\xi}) = \frac{1}{2}\dot{\hat{u}}_j^c(\boldsymbol{\xi}) + \int_{\Gamma^n} \left[U_{ij}(\boldsymbol{\xi},\boldsymbol{x})\,\dot{t}_j^n(\boldsymbol{x}) - T_{ij}(\boldsymbol{\xi},\boldsymbol{x})\,\dot{u}_j^n(\boldsymbol{x})\right]\,d\Gamma^n(\boldsymbol{x}) + \int_{\Gamma^c} \left[U_{ij}(\boldsymbol{\xi},\boldsymbol{x})\,\dot{\hat{t}}_j^c(\boldsymbol{x}) - T_{ij}(\boldsymbol{\xi},\boldsymbol{x})\,\dot{\hat{u}}_j^c(\boldsymbol{x})\right]\,d\Gamma^c(\boldsymbol{x}) \quad (3)$$

is evaluated. The crack surface interaction leads to additional contact tractions t_i^{cont} at the crack such that the total tractions read as $t_i = t_i^{load} + t_i^{cont}$. Without loss of generality, initially unloaded cracks are considered in the present paper, $t_i^{load} = 0$. Due to the action-reaction principle the contact tractions are equal according to the amout but with opposite sign. Therewith, the discontinuities of the tractions vanish, $\hat{t}_i^{cont} = 0$.

For the solution of the contact problem the penalty method in the framework of a radial return mapping algorithm [8] is applied. Within this method small, relative, reversible displacements $\hat{u}^{c,rev}$ of the contact surfaces are allowed. In the present context the contact tractions are linked to these displacement discontinuities via a constant normal ρ_n and tangential ρ_t stiffness, $t_n^c = \rho_n \hat{u}_n^c, \quad t_{t_i}^c = \rho_t \hat{u}_{t_i}^{c,rev}$.

In case of slip irreversible, tangential displacement discontinuities $\hat{u}_{t_i}^{c,irr}$ have to be considered. Therefore, an additive decomposition of the tangential displacement discontinuities into a reversible $\hat{u}_{t_i}^{c,rev}$ and an irreversible $\hat{u}_{t_i}^{c,irr}$ part is applied, $\hat{u}_{t_i}^c = \hat{u}_{t_i}^{c,rev} + \hat{u}_{t_i}^{c,irr}$.

For the detection of the slip state, Coulomb's frictional law is utilized.

CRACK GROWTH ALGORITHM

Based on the results of the stress analysis the new crack front is generated in three steps as shown in Fig. 2.

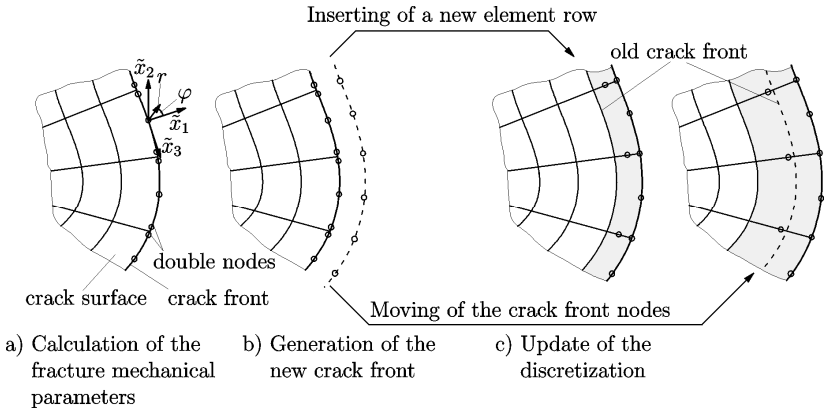

Figure 2. Three steps of an increment

First, the stress intensity factors (SIFs) are calculated for each time step. For discrete points along the crack front (see Fig. 2a) the SIFs and T-stresses are calculated from the stress near field by an extrapolation method. The results of the utilized regression analysis are optimized by the minimization of the standard deviation [3]. For points P_i at a smooth crack front the typical stress distribution is given by [9]:

$$\sigma_{ij}(r,\varphi,P) = \sum_{M=I}^{III} \frac{K_M(P)}{\sqrt{2\pi r}} f_{ij}^M(\varphi) + T_{ij}(P) + O(\sqrt{r}) . \tag{4}$$

The SIFs K_M ($M = I,II,III$) characterize the intensity of the typical square root singularity while T_{ij} denote the T-stresses. $f_{ij}^M(\varphi)$ are the angular functions corresponding to the mode M. The cyclic equivalent SIF $\Delta K_{eq}(P)$ is determined by the analysis of a representative load cycle via $\Delta K_{eq}(P) = K_{eq}(P,t_{up}) - K_{eq}(P,t_{lo})$. The time, when the maximum equivalent SIF is present, is denoted by t_{up} and t_{lo} is the time, when the minimum equivalent SIF is present. According to the cyclic equivalent SIF the cyclic SIFs $\Delta K_M(P)$ are defined by $\Delta K_M = K_M(P,t_{up}) - K_M(P,t_{lo})$.

In the second step the new position of the crack front is determined by the evaluation of a suitable crack growth criterion based on the SIFs. The obtained crack extension as well as the kink angle define the new position of the point P_i, cf. Fig. 2b. The new positions of the crack front points set up the new crack front.

Finally, the gap between the old and the new crack front has to be closed [10]. Two possibilities are available. On the one hand a new row of elements is inserted. This is a good choice if there are significant crack extensions for example in case of predictor

steps. On the other hand in case of corrector steps only small crack extensions along the whole crack front occur. Therefore, the nodes of the old crack front are moved towards the new crack front.

PREDICTOR CORRECTOR SCHEME

Starting from an initial crack front a new one is predicted. Since only the state of stress and strain of the initial crack front is known, the prediction is performed in a linear way. Due to this linearization an error has been made. By the consideration of the stress state of the predicted crack front, this error can be estimated and the crack front can be corrected with respect to its shape and location.

Predictor

For the determination of the crack extension $\Delta a(P^A)$ for a point P^A at the initial crack front (superscript *A*) a crack propagation rate e.g. the Paris law is evaluated for a user-specified numer of load cycles ΔN_{lc}:

$$\Delta a(P^A) = \left(\frac{da}{dN}\left(\Delta K_{eq}(P^A)\right)\right)\Delta N_{lc}\,. \tag{5}$$

The crack deflection $\Delta\varphi(P^A)$ is calculated by the maximum tangential stress criterion [5]. In the present case of non-proportional mixed mode conditions the SIFs are replaced by the ranges of the SIFs [6]:

$$\Delta\varphi(P^A) = 2\arctan\left(\frac{-2\,\Delta K_{II}(P^A)}{\Delta K_I(P^A) + \sqrt{\Delta K_I^2(P^A) + 8\,\Delta K_{II}^2(P^A)}} \right). \tag{6}$$

Corrector

In the next incremental loop the state of stress at the predicted crack front (superscript *B*) is additionally known. Therewith, the cyclic equivalent SIF is approximated between the initial and the predicted crack front according to its general definition by [4]

$$\Delta K_{ey}^{app}(a, P^A) = \Delta K_{eq}(P^A)\sqrt{\frac{a}{a_0(P^A)}}, \quad a_0(P^A) \le a(P^A) \le a_0(P^A) + \Delta a(P^A) \tag{7}$$

with the virtual initial crack length

$$a_0(P^A) = \Delta a(P^A)\frac{\Delta K_{eq}^2(P^A)}{\Delta K_{eq}^2(P^B) - \Delta K_{eq}^2(P^A)} \tag{8}$$

P^B is the location of the point P^A at the predicted crack front. Therewith, the number of load cycles is re-calculated via

$$\Delta N_{re}(P^A) = \int_{a_0}^{a_0+\Delta a} \frac{1}{\frac{da}{dN}(\Delta K_{eq}^{app}(a, P^A))} da \tag{9}$$

and the predicted crack extension is replaced by

$$\Delta a_{corr}(P^A) = \Delta a(P^A) + \left(\frac{da}{dN}\left(\Delta K_{eq}(P^A)\right)\right)\left(\Delta N_{lc} - \Delta N_{re}(P^A)\right). \tag{10}$$

until the relative error $\left|\Delta N_{lc} - \Delta N_{re}(P^A)\right| / \Delta N_{lc}$ is smaller than a user-specified tolerance. By the consideration of the direction of crack growth $\Delta\varphi(P^B)$ at the predicted crack front the corrected crack deflection is obtained by

$$\Delta\varphi_{corr}(P^A) = \frac{K_{eq}(P^A)\Delta\varphi(P^A) + K_{eq}(P^B)\Delta\varphi(P^B)}{K_{eq}(P^A) + K_{eq}(P^B)}. \tag{11}$$

EXAMPLES

The first example is chosen to investigate the required number of load cycles for the simulation in order to obtain a characteristic one for the fracture mechanical analysis. The second example shows the influence of friction on the crack path.

Single edge crack specimen

A beam with a rectangular cross section as shown in Fig. 3a with an edge crack at half of the length is taken into account. The beam consists of the material steel (*E=210 GPa, v=0.3*) and it is loaded by a time-invariant compressive force *F* and a time-depending torsional moment *T(t)*. In Fig. 3b the loadings versus time are ploted.

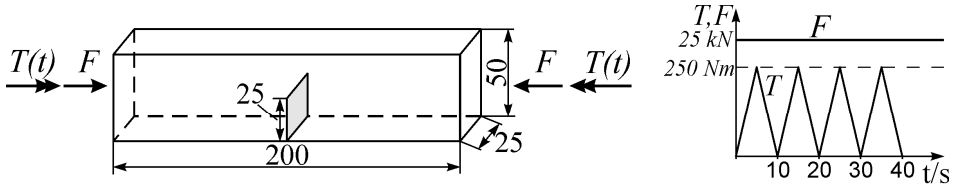

a) geometry and loading b) loading process

Figure 3. geometry and loading of SEC-specimen.

The stress analysis has been carried out for different frictional coefficients μ. The resulting hysteresis curves of the K_{III}-value at the middle of the crack front are illustrated in Fig. 4.

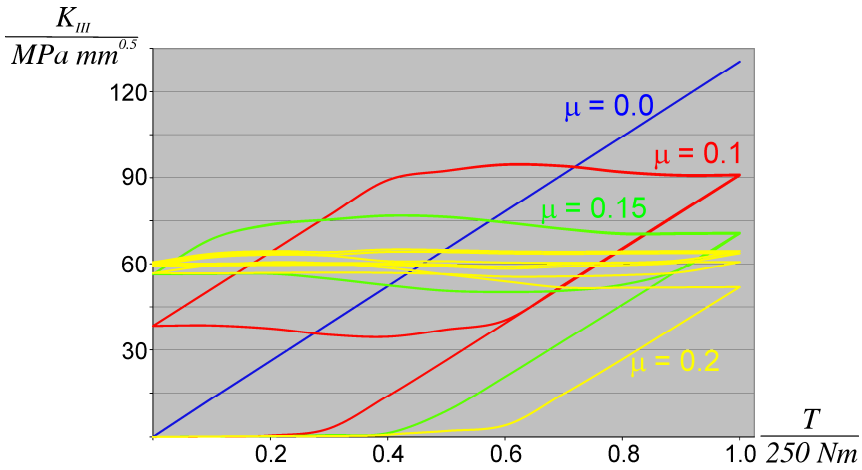

Figure 4. hysteresis curves.

For μ=0 the SIF is directly linked to the loading moment. In case of small frictional coefficients (μ=0.1 and μ=0.15) steady behavior is already observed after the frist load cycle. For μ=0.2 at least three load cycles are required until steady behavior is present.

Overall, the SIF oscilates around the constant mean value of *65 MPa* $mm^{0.5}$ with a decreasing amplitude for an increasing frictional coefficient.

Compressive Specimen

A plate as scetched in Fig. 5a with a plane initial crack, that is slanted by *45°* to the mid-cross section, is loaded by a compressive force *F* , which oscilates between *100 kN* and *200 kN*, cf. Fig. 5b.

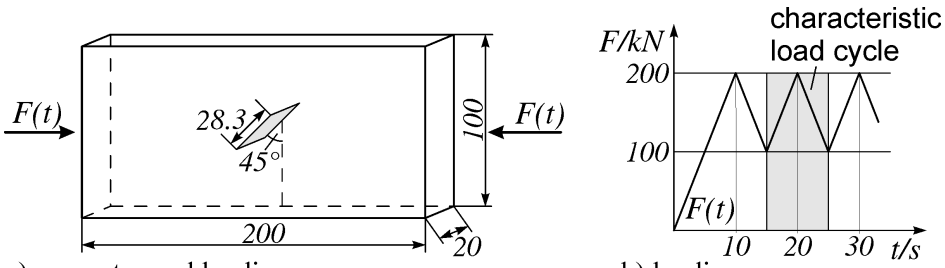

Figure 5. geometry and loading of plate

The specimen consists of the material steel with the Young's modulus *E=210 GPa* and the Poission ratio ν=0.3. For the simulation of crack propagation the Paris law is utilized:

$$\frac{da}{dN} = 1.27 \cdot 10^{-12} \left(\frac{\Delta K_{eq}}{MPa\, mm^{0.5}} \right)^{2.66} . \qquad (12)$$

The simulation has been carried out with the frictional coefficients μ=0.0 and μ=0.1. Figure 6 shows the resulting crack paths.

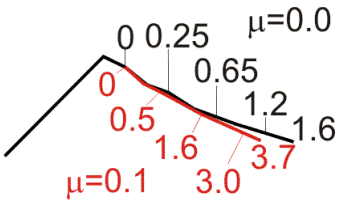

Figure 6. Crack path with number of load cycles in millions.

The crack paths of both simulations are approximately identical. However, obvious differences concerning the number of load cycles can be observed. In both simulations the cyclic stress intensity factor is decreasing while the crack is growing.

REFERENCES

1. Portella, A., Aliabadi, M.H., Rooke, D.P. (1992) In: *International Journal for Numerical Methods in Engineering* **33**, pp.1269-1287.
2. Partheymüller, P., Haas, M., Kuhn, G. (2000) In: *Engineering Analysis with Boundary Elements* **24**, pp.777-788, Elsevier, Netherlands.
3. Kolk, K. (2005) *Automatische 3D-Rissfortschrittssimulation unter Berücksichtigung von 3D-Effekten und Anwendung schneller Randelementformulierungen*, VDI-Verlag, Düsseldorf.
4. Weber, W., Steinmann, P., Kuhn, G. (2008) In: *Journal of Fracture* **149**, pp. 175-192, Springer.
5. Erdogan, F., Sih, G. (1963) In: *Journal of basic engineering* **85**, pp. 519-525, ASME Transactions.
6. Tanaka, K., Akiniwa, Y., Wakita, S. (2006) In: *Proceedings of International Conference on crack paths (CP2006)*, Parma, Italy.
7. Weber, W., Kuhn, G. (2007) In: *Engineering Fracture Mechanics* **75**, pp.452-460, Elsevier, Netherlands.
8. Willner, K. (2003) *Kontinuums- und Kontaktmechanik*, Springer, Berlin.
9. Leblond, J., Torlai, O. (1992) In: *International Journal of Elasticity* **29**, pp.97-131.
10. Kolk, K., Kuhn, G. (2005) In: *Fatigue and Fracture of Engineering Materials and Structures* **28**, pp.117-126, Blackwell Publishing Ltd.